Available online at www.sciencedirect.com

ScienceDirect

journal homepage: www.elsevier.com/locate/he

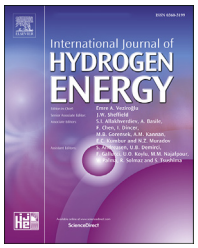

SOFC anodes impregnated with noble metal catalyst nanoparticles for high fuel utilization

Shotaro Futamura [a], *Aki Muramoto* [a], *Yuya Tachikawa* [a,b,c], *Junko Matsuda* [b,d], *Stephen M. Lyth* [d,e], *Yusuke Shiratori* [a,c,f], *Shunsuke Taniguchi* [b,c,f], *Kazunari Sasaki* [a,b,c,d,e,f,*]

[a] *Department of Hydrogen Energy Systems, Faculty of Engineering, Kyushu University, Motooka 744, Nishi-ku, Fukuoka, 819-0395, Japan*

[b] *Center of Coevolutionary Research for Sustainable Communities, Kyushu University, Motooka 744, Nishi-ku, Fukuoka, 819-0395, Japan*

[c] *Next-Generation Fuel Cell Research Center (NEXT-FC), Kyushu University, Motooka 744, Nishi-ku, Fukuoka, 819-0395, Japan*

[d] *International Institute for Carbon-Neutral Energy Research (WPI-I2CNER), Kyushu University, Motooka 744, Nishi-ku, Fukuoka, 819-0395, Japan*

[e] *Platform of Inter / Transdisciplinary Energy Research (Q-PIT), Kyushu University, Motooka 744, Nishi-ku, Fukuoka, 819-0395, Japan*

[f] *International Research Center for Hydrogen Energy, Kyushu University, Motooka 744, Nishi-ku, Fukuoka, 819-0395, Japan*

ARTICLE INFO

Article history:
Received 26 October 2018
Received in revised form
21 January 2019
Accepted 24 January 2019
Available online 6 March 2019

Keywords:
Solid oxide fuel cell
La-doped $SrTiO_3$
Noble metal catalyst impregnation
High fuel utilization stability

ABSTRACT

Redox-stable solid oxide fuel cell (SOFC) anodes are developed in order to improve durability at higher fuel utilization, as a possible alternative to conventional Ni-zirconia cermet anodes. $Ce_{0.9}Gd_{0.1}O_2$ (GDC) is utilized as a mixed ionic and electronic conductor (MIEC), in combination with $Sr_{0.9}La_{0.1}TiO_3$ (LST) as an electronic conductor. The stability of noble metals (Rh, Pt, and Pd) is analyzed via thermochemical calculation of stable phases. Noble metal catalyst nanoparticles are incorporated via co-impregnation with GDC. The electrochemical characteristics of SOFC single cells using these anode materials are investigated in highly-humidified H_2 at 800 °C. Their stability at high fuel utilization is analyzed. These co-impregnated anodes with highly dispersed noble metal catalysts on the LST-GDC conducting backbones, achieve high I–V performance comparable to conventional Ni-cermet anodes. The co-impregnated anodes also achieve considerably high catalytic mass activity. At higher oxygen partial pressure, where the Ni catalyst can be deactivated by oxidation, these noble catalysts are thermochemically stable in the metallic state, and tolerant against oxidation. This class of alternative catalyst, impregnated with low-loading of noble metals could contribute to stable operation in the downstream region of SOFC systems. A simple cost analysis indicates a tolerance of using noble metals, provided their loading is sufficiently low.

* *Corresponding author*. Kyushu University, Next-Generation Fuel Cell Research Center, Motooka 744, Nishi-ku, Fukuoka, 819-0395, Japan.
E-mail address: sasaki@mech.kyushu-u.ac.jp (K. Sasaki).

https://doi.org/10.1016/j.ijhydene.2019.01.223

Introduction

SOFCs are promising electrochemical energy conversion systems that are operated at high temperatures, typically between 600 and 900 °C. The high operating temperature leads to several advantages, including high electrical conversion efficiency, fuel flexibility, and fabrication without the need for noble metal catalysts [1–6]. In Japan, for example, more than 250,000 fuel cell units have been sold by July 2018 as residential co-generation power systems. Whilst the commercialization of such systems began with polymer electrolyte fuel cells (PEFCs), an increasing proportion of these are now based on SOFCs [6]. Widespread commercialization of SOFCs has also started for industrial applications, and SOFC systems combined with micro gas turbines and/or steam turbines can achieve high electric efficiency [6]. Thus, SOFCs are expected to make a great contribution to the realization of highly efficient energy systems in the future [1–6].

The nickel-zirconia cermet has been widely used as a conventional SOFC anode material for decades. The porous microstructure has a large triple-phase boundary (TPB) where the electrode reactions can occur. However, the Ni-based electron-conducting backbones can be easily destroyed by Ni/NiO redox reactions, especially during e.g. system shutdown and fuel supply interruption, leading to severe performance degradation, due to e.g. possible inhomogeneous supply of fuel at high fuel utilization (i.e. under high vapor pressure) [7–12]. Many papers have discussed the disadvantages of conventional Ni-cermet anodes under redox cycling, and such anodes are also likely to deteriorate even under conditions of high steam pressure. For example, Holzer et al. [8] reported that coarsening of Ni is accelerated in the presence of water vapor. In addition, Kawasaki et al. [11] analyzed degradation due to Ni oxidation with the anode voltage below the Ni/NiO coexistence boundary, at high fuel utilization. Higher efficiency is required for widespread commercialization of SOFCs in the future, and therefore tolerance of high fuel utilization is desired.

Conducting oxides with perovskite structure, ABO_3, have received much attention as alternative SOFC anode materials. Strontium titanate ($SrTiO_3$) in particular has been found to have excellent chemical and physical stability in both oxidizing and reducing atmospheres under SOFC operating conditions. Sufficiently high electrical conductivity can be achieved in this material by controlling cation doping (e.g. by doping with La, or Y at the A-site) [13–18]. Marina et al. [13] and Wang et al. [17] have both reported the thermal and electrochemical properties of $(La_xSr_{1-x})TiO_3$ (LST). Meanwhile, Obara et al. [14] and Li et al. [15] analyzed the electrochemical properties of $(Y_xSr_{1-x})TiO_3$ (YST), and Ma et al. [18] showed that the conductivity of LST was better than that of YST. These studies have shown that such materials are promising as alternative anode materials. In addition, several other researchers have evaluated SOFC anodes composed of LST or YST instead of Ni [19–24]. Whilst these alternative anode materials have shown excellent tolerance against redox cycling, the catalytic activity of these conductive oxides is not sufficient compared to Ni metal. Impregnation (or infiltration) is a technique that has been widely used in order to obtain dispersed catalyst particles on ceramic support materials [20–25]. Ni metal catalyst or GDC nanoparticles have been loaded onto conducting oxide backbones via impregnation, to improve their catalytic activity. Yoo et al. [21,22] and Shen et al. [24,25] reported both high tolerance and improvement of the catalytic activity by preparing highly-dispersed Ni catalysts on LST conducting backbones. Moreover, several research groups have studied the exsolution of metal catalyst particles from LST perovskite materials [20,26–28]. This method is to incorporate the catalyst as a dopant within the host perovskite lattice during synthesis in air, which is then in situ exsolved at the surface as a catalytically active metal nanoparticle under reducing conditions. Irvine et al. reported that catalyst particles grown by redox exsolution could improve the electrochemical activity and tolerance against carbon deposition [20,26,27].

We have developed an alternative SOFC anode, in which Ni and GDC catalyst particles are dispersed on conducting oxide backbones composed of LST (an electron conductor) and GDC (a mixed ionic and electronic conductor, MIEC) [29,30], forming a thin two-dimensional Ni-GDC cermet structure supported on a stable conductive LST-GDC backbone. While typical SOFC anodes have a three-dimensional interpenetrating structure consisting of ionic (or mixed) conductor, electronic conductor, and pores, this thin supported Ni-GDC cermet could also prevent aggregation of Ni particles, resulting better electrochemical activity and stability against coarsening compared to Ni catalysts impregnated without the presence of GDC [29]. The catalyst particles are deposited by impregnation rather than exsolution, in order to keep them on the oxide backbones even at high fuel utilization, or under relatively oxidizing conditions. This anode not only has high tolerance against redox cycling, but also initial electrochemical performance comparable to conventional three-dimensional Ni-cermet anodes. Thus, this is a promising alternative anode for robust operation of SOFC systems at high fuel utilization. In the downstream region of SOFC systems at high fuel utilization, conductive oxide backbones are generally stable against oxidation. However, the highly-dispersed Ni catalyst nanoparticles can be deactivated by oxidation due to the low anode potential at higher oxygen partial pressure in steam-rich fuels. Thus, Ni-free stable catalysts should be developed for operation at high fuel utilization.

Several studies have been conducted reporting the catalytic activity of noble metals, such as Ru, Rh, Pd, or Pt for the reforming of hydrocarbon fuels [31–33]. These noble metal catalysts have stability against carbon deposition as well as high reforming activity, and they are indeed utilized in commercial reforming systems. Provided that they are used at low loading via e.g. impregnation, or exsolution, they may be useful and cost-efficient not only as reforming catalysts, but also as anode catalysts in SOFCs (similar to the Pt electrocatalyst for PEFCs). Indeed, PEFC systems with low Pt loading have already been commercialized for stationary and automobile applications such as private vehicles and forklifts [5,6]. Some researchers have evaluated the electrochemical activities of these noble metals in SOFC anodes [34–39]. For example, Gorte et al. analyzed the electrochemical activities and carbon tolerance of precious metals of SOFC anodes for

reforming of CH_4 [35,37]. Whilst several other researchers have also reported the stability against carbon deposition and electrochemical activity of noble metal catalysts, few papers have analyzed their electrochemical characteristics and stabilities at high fuel utilization.

Here, we combine GDC as a MIEC, with LST as electronic conductor, to prepare a redox-stable SOFC anode backbone. This material is used as an alternative to conventional Ni-cermet anodes in zirconia-based electrolyte-supported SOFCs. The concept of this study is to fabricate a robust anode backbone using oxide conductors, on which electrochemically-active catalysts are dispersed. Noble metal catalysts with thermochemical stability, such as Rh, Pt, and Pd, are dispersed on these conducting backbones via co-impregnation with GDC, to form thin, supported cermet. The electrochemical characteristics and stability of SOFC single cells using these alternative anodes are investigated in highly-humidified H_2 at 800 °C. The aim of this study is to develop alternative SOFC anodes for high fuel utilization, with noble metal catalysts as alternative anode catalysts to Ni, tolerant against oxidation even in the downstream region of SOFC systems with relatively high oxygen partial pressure in the fuels. Since one of the advantages of SOFC is their avoidance of the use of noble metals in general, a cost analysis is performed to confirm the viability of using these noble metals.

Thermochemical calculations

Thermochemical calculations were carried out using HSC-Chemistry software (Version 9.0.5, Outkumpu Research Oy, Finland), with an extensive thermochemical database. Here,

Table 1 – Chemical species containing Ni, Rh, Pt, or Pd taken into account in the thermochemical calculations.

Element	Chemical species considered in thermochemical calculations
Ni	Ni(g), Ni_2(g), NiH(g), NiO(g), NiOH(g), $Ni(OH)_2$(g), Ni_3C, $NiCO_3$, $NiCO_3 \cdot 5.5H_2O$, NiO, $Ni(OH)_2$, $Ni(OH)_3$, $Ni_2O_3 \cdot 3H_2O$, Ni
Rh	Rh(g), RhC(g), RhO(g), RhO_2(g), RhO, RhO_2, Rh_2O, Rh_2O_3, Rh
Pt	Pt(g), PtC(g), PtH(g), PtO(g), PtO_2(g), PtO, PtO_2, Pt_3O_4, Pt $(OH)_2$, Pt
Pd	Pd(g), PdO(g), PdO, $Pd(OH)_2$, $Pd(OH)_4$, $PdO_2 \cdot 2H_2O$, Pd

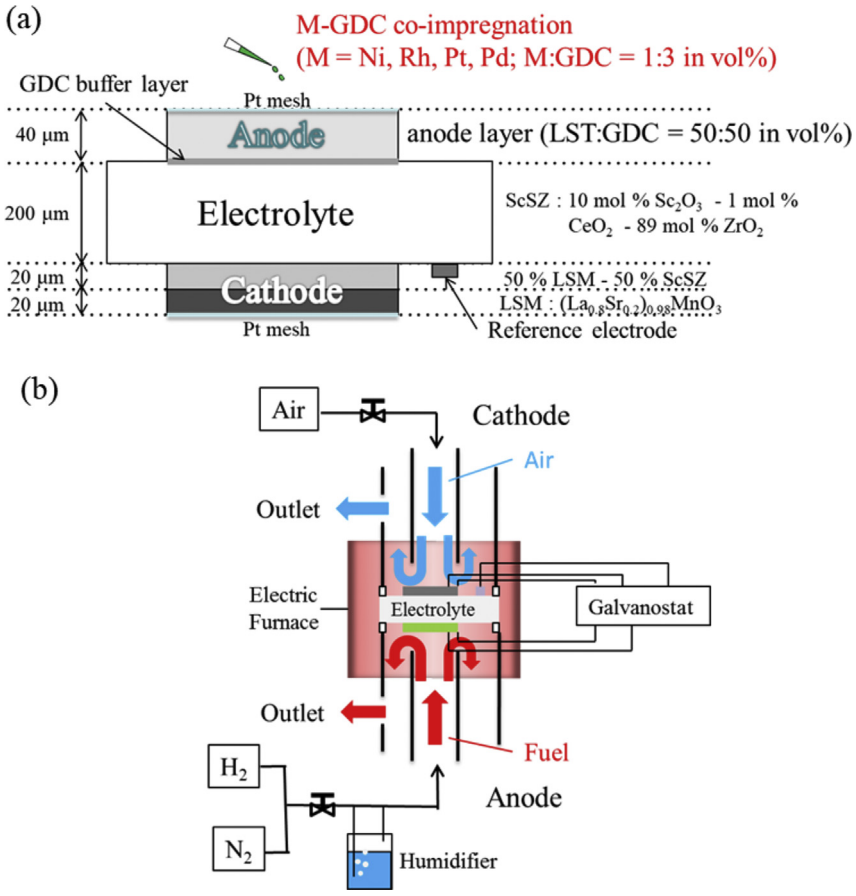

Fig. 1 – Schematic drawings of (a) the SOFC single cell with an LST-GDC backbone, and (b) the experimental setup for electrochemical measurements.

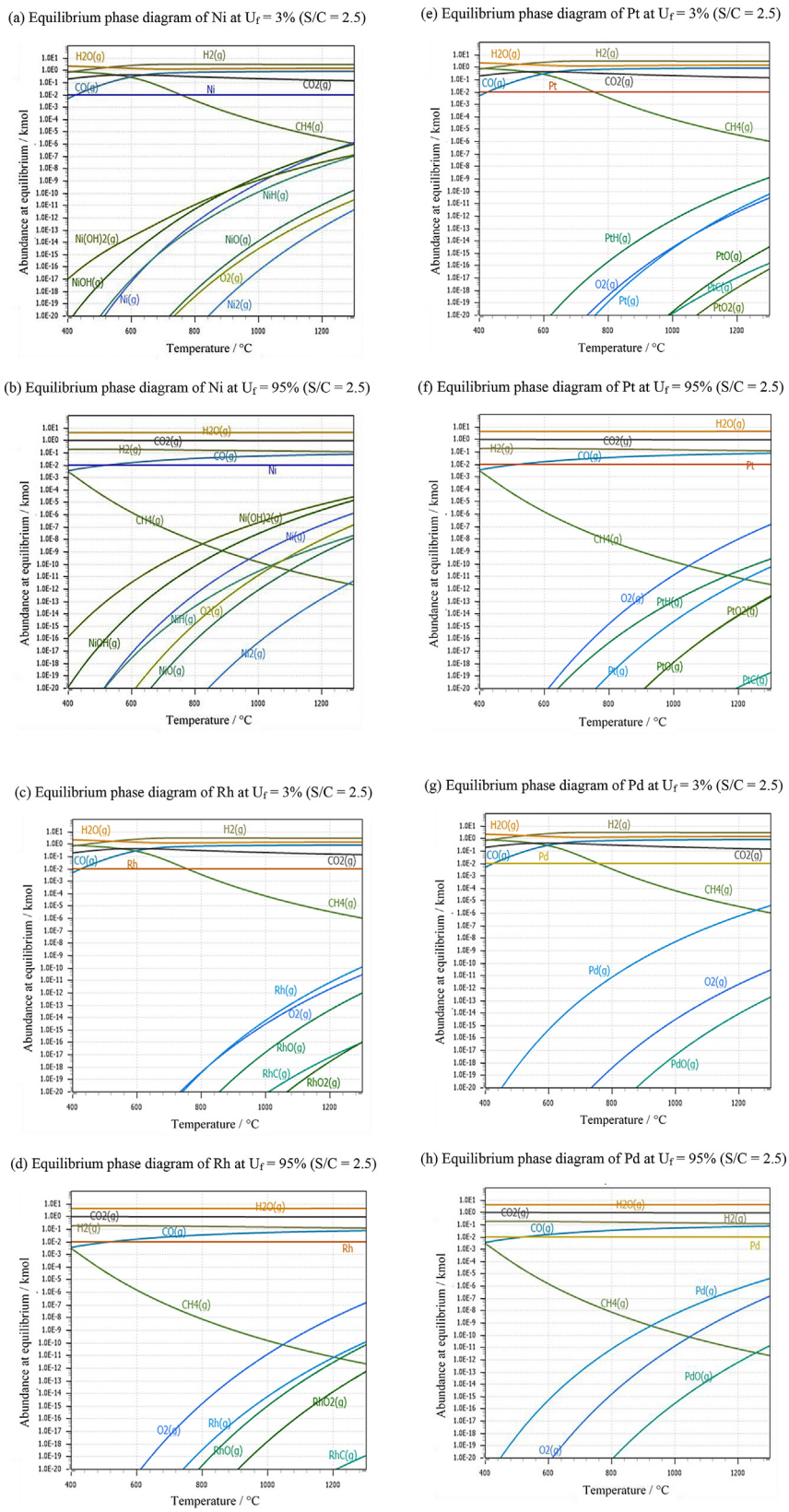

Fig. 2 – Equilibrium phase diagrams for M, where M = (a, b) Ni, (c, d) Rh, (e, f) Pt, and (g, h) Pd. Fuel utilization of (a, c, e, g) 3% and (b, d, f, h) 95% were used at S/C = 2.5.

the thermochemical data of the verified major constituents of fuels used in SOFCs (i.e. H_2(g), O_2(g), H_2O(g), CO(g), CO_2(g), CH_4(g), and graphite) were considered [40,41]. The M-containing species (M = Ni, Rh, Pt, and Pd) taken into account in the anode are shown in Table 1. Calculations were performed assuming a reactor containing 0.01 kmol M (M = Ni(s), Rh(s), Pt(s), or Pt(s)), to which 1 kmol of CH_4 gas and 2.5 kmol of H_2O were supplied (i.e. a steam-to-carbon ratio (S/C) of 2.5), and the calculation was conducted for various fuel utilizations (U_f), by numerically adding oxygen into the fuels. The amounts of gas or solid products in thermochemical equilibria were numerically derived in the temperature range between 400 and 1300 °C in steps of 10 °C. The total pressure was set to be 1 bar. The amount of each product in thermochemical equilibria was derived via the Gibbs free energy minimization method [40,41]. Some thermochemical data are only available within a limited temperature range, so that such data were extrapolated to the temperature range calculated when necessary.

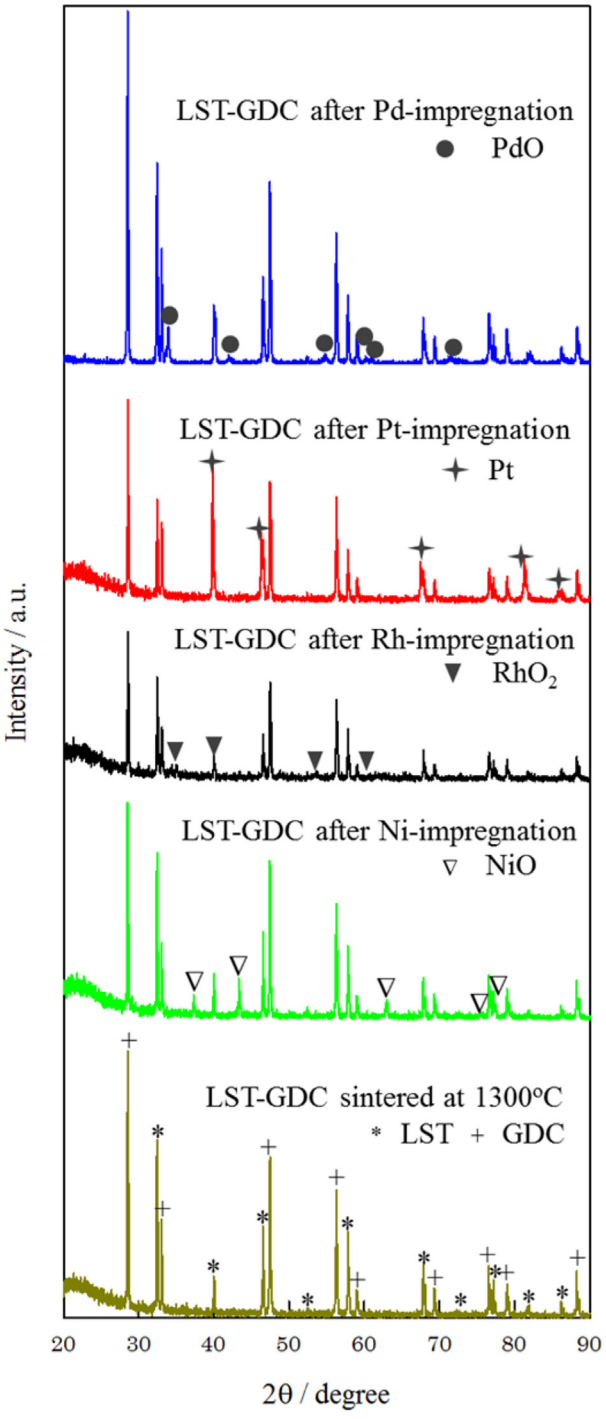

Fig. 3 – X-ray diffraction patterns for pre-sintered LST-GDC after M-impregnation (M = Ni, Rh, Pt, or Pd) and following thermal treatment in air at 1000 °C for 2 h.

Experimental

Cell fabrication

Fig. 1(a) shows a schematic diagram of the SOFC single button cell used in this study. Scandia-stabilized zirconia (ScSZ) plates (10 mol% Sc_2O_3, 1 mol% CeO_2, and 89 mol% ZrO_2, Daiichi Kigenso Kagaku Kogyo Co., Ltd., Osaka, Japan) with a diameter of 20 mm and a thickness of 200 μm were used as the solid electrolyte. Anode powders were prepared by mixing LST ($La_{0.1}Sr_{0.9}TiO_3$, Praxair, Inc., CT, USA) and GDC ($Gd_{0.1}Ce_{0.9}O_2$, Rhodia, ULSA grade, USA) in a 50:50 ratio by volume. Anode paste was prepared by blending the anode powders with organic binder (α-terpineol). Cathode paste for the functional layer was made with lanthanum strontium manganite (LSM, $(La_{0.8}Sr_{0.2})_{0.98}MnO_3$, Praxair, USA) and ScSZ powders in a 47:53 ratio by volume. The current-collecting cathode layer comprised LSM powder [10].

A thin buffer layer of GDC with a thickness of around 5 μm, was deposited at the interface between the anode and the electrolyte, followed by sintering in air at 1400 °C for 2 h. This buffer layer was used to prevent LST from reacting with zirconia-electrolyte to form electrically resistive secondary products such as $SrZrO_3$ at high temperature [29]. Porous anode layers (with porosity of around 33%) were then screen-printed onto the buffer layer on ScSZ electrolyte plates, followed by sintering in air at 1300 °C for 3 h. Cathode layers were screen-printed onto the counter side of the ScSZ electrolyte plates, followed by sintering in air at 1200 °C for 5 h. The porosity of the first LSM-ScSZ layer was around 22%, and that of the second LSM layer was around 29%. Fig. 1(a) shows the thickness of each layer after sintering. The thickness and geometric area of the electrode layers were approximately 40 μm and 8 × 8 mm^2 (0.64 cm^2), respectively.

For co-impregnation, the prepared porous anode layer was then soaked with an aqueous M-GDC (M = Ni, Rh, Pt, or Pd) dispersion: a co-impregnation solution of $Ni(NO_3)_2{\cdot}6H_2O$ (Kishida Chemicals Co. Ltd., Japan), $RhCl_3{\cdot}nH_2O$ (Kishida Chemicals Co. Ltd., Japan), $H_2PtCl_6{\cdot}6H_2O$ (Kishida Chemicals Co. Ltd., Japan), or $Pd(NO_3)_2{\cdot}nH_2O$ (Kishida Chemicals Co. Ltd., Japan), $Gd(NO_3)_3{\cdot}6H_2O$ (Kanto Chemical Co., Inc., Japan) and $Ce(NO_3)_3{\cdot}6H_2O$ (Kishida Chemicals Co., Ltd., Japan). Each metal catalyst loading was 0.167 mg-Ni cm^{-2}, 0.178 mg-Rh cm^{-2}, 0.310 mg-Pt cm^{-2}, and 0.204 mg-Pd cm^{-2}, respectively. This co-impregnation procedure was made with a GDC in a mixing volume ratio of M:GDC = 1:3, followed by thermal

decomposition of these precursors in air at 1000 °C for 2 h, to obtain metal or metal oxide nanoparticles and GDC, loaded on the electrode backbone. Phase identification of the synthesized SOFC anode materials was performed by X-ray diffraction analysis (XRD with Cu Kα radiation) (Rigaku RINT Ultima III, Japan).

For single button cells, a reference electrode (RE) with a geometric area of 0.04 cm^2 was then painted 2 mm away from the edge of the cathode, using Pt paste (U-3401, Metalor Technologies Japan). Since the anode potential was measured between the anode, and the reference electrode on the cathode side, it has a higher value than the cell voltage by the potential difference between the cathode and the reference electrode, due to the cathodic overvoltage. Pt mesh (80 mesh acting) was attached to each electrode surface as a current collector.

Cell test

Fig. 1 (b) shows the electrochemical experimental setup. Before measuring the electrochemical characteristics, the cell was heated up to 1000 °C at a rate of 200 °C h^{-1}, in order to melt the Pyrex glass powder and seal the cell. 3%-humidified H_2 gas was subsequently supplied to the anode for 1 h at 100 mL min^{-1}, in order to reduce metal oxide to metallic catalyst. Cell performance (I–V characteristics, anode IR losses, and anode non-ohmic overvoltage) was measured at 800 °C utilizing differently humidified hydrogen gas for the anode, and dry air at 150 mL min^{-1} for the cathode. The anode voltage was measured as the voltage between the anode and the cathode-side reference electrode. The anode-side voltage losses were divided into anode IR losses and anode non-ohmic overvoltage using the well-known current interruption technique [10,42].

High fuel utilization test

High fuel utilization tests were performed to simulate the downstream conditions in practical SOFC systems. For improved efficiency, it is desired to realize operation at higher fuel utilization (U_f). To simulate such conditions in the downstream region of systems operated at U_f = 95%, 95%-

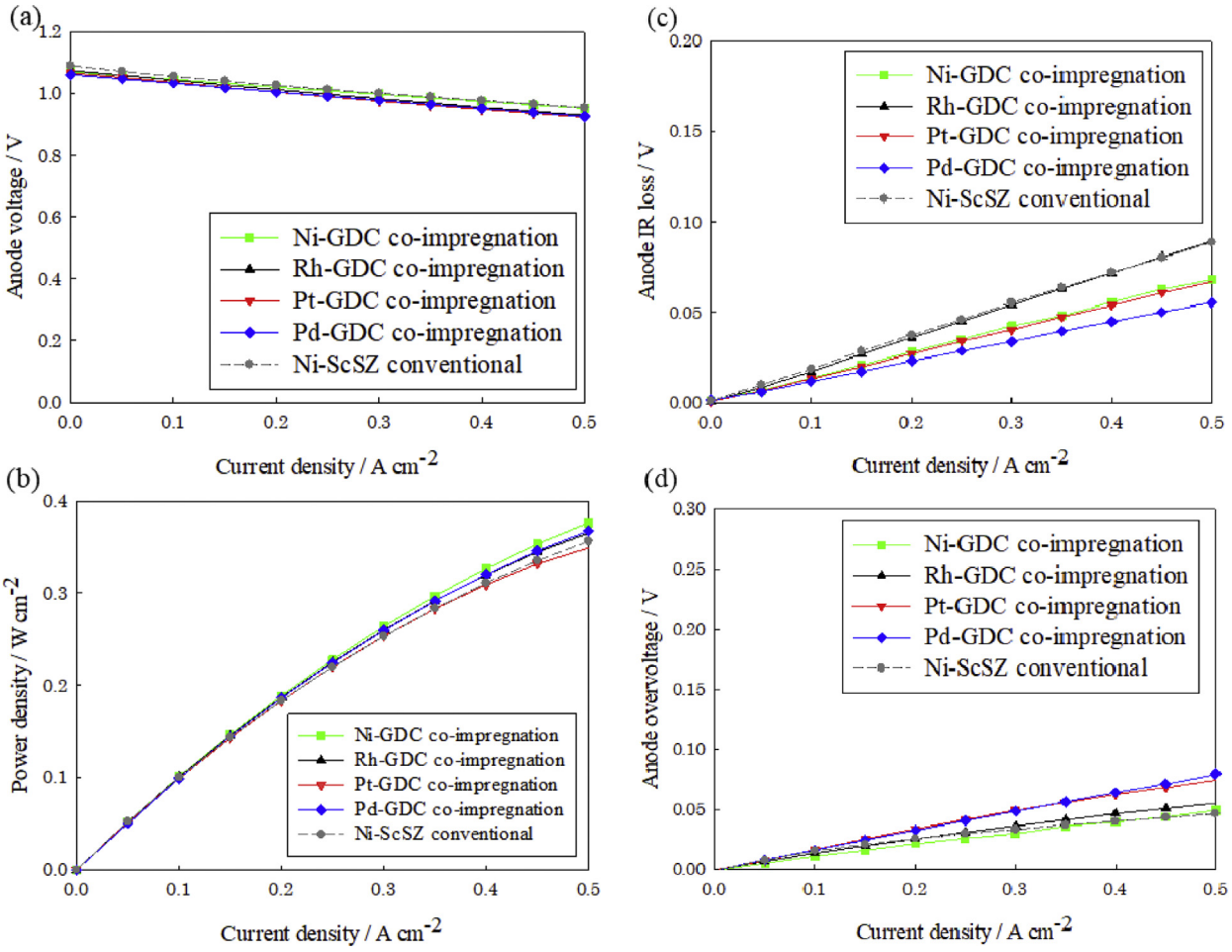

Fig. 4 – (a) Anode voltage, (b) cell power density, (c) anode IR losses, and (d) anode non-ohmic overvoltage of M-impregnated anodes (M = Ni, Rh, Pt, or Pd) and conventional Ni-cermet anodes with 3%-humidified H_2 fuel. Metal catalyst loadings are 0.167 mg-Ni cm^{-2}, 0.178 mg-Rh cm^{-2}, 0.310 mg-Pt cm^{-2}, and 0.204 mg-Pd cm^{-2}, respectively.

humidified hydrogen gas was used as a model fuel to a single cell, and the anode voltage was measured at a constant current density of 0.2 A cm^{-2}.

Microstructural observation

A field-emission scanning electron microscope, coupled with energy-dispersive X-ray analysis (FESEM-EDS, Hitachi High-Technologies, S-5200, EDAX genesis 4000/JSM-700IF JEOL, Japan) and a focused-ion beam system coupled with a scanning electron microscope (FIB-SEM, HeliosNanolab 600i, FEI, USA) were applied to observe and analyze the anode microstructures. The 3D microstructures were reconstructed from FIB-SEM images using the software "Amira" (version 6.0, FEI, USA).

Exchange current density at anodes

Exchange current density values are useful to phenomenologically quantify SOFC electrode characteristics. The following Butler-Volmer-type equation may be used to approximate the empirical relationship between current density and electrode polarization [3,43].

$$i = i_0\left\{\exp\left(\frac{\alpha_a nF\eta}{RT}\right) - \exp\left(\frac{\alpha_c nF\eta}{RT}\right)\right\} \quad (1)$$

In this equation, i, i_0, and η are the current density, the exchange current density, and the electrode polarization, respectively. α_a and α_c are the anodic and cathodic transfer coefficients, respectively. In addition, n, R, T are the number of electrons participating in the electrode reaction, the gas constant, and the absolute temperature, respectively. In this study, the average of the anodic exchange current density was derived from the measured current density between 0.25 A cm^{-2} and 0.40 A cm^{-2} by assuming that $\alpha_a = \alpha_c = 0.5$, and that $n = 2$.

Results and discussion

Thermochemical stability

Thermochemical calculations are useful in deriving the major phase and possible minor phases causing sublimation. Fig. 2 shows equilibrium phase diagrams for 0.01 kmol M (M = Ni, Rh, Pt, or Pd) in 1 kmol CH_4 and 2.5 kmol H_2O (i.e. S/C = 2.5) at low fuel utilization (3%) and high fuel utilization (95%), i.e., 3% or 95% of the fuel is assumed to be oxidized (i.e. consumed), respectively. The abundance at equilibrium is shown in a logarithmic scale. Fig. 2(a) shows that, among the different possible phases of nickel and nickel compounds (0.01 kmol in total), Ni(s) is the most stable (i.e. the most abundant) under reducing conditions at both low (3%) and high (95%) fuel utilization. The presence of NiO(s) is only observed in the calculations if U_f exceeds 98% (i.e. in >98%-humidified H_2 fuel). The abundance of gaseous species at equilibrium, such as $Ni(OH)_2$(g) and NiOH(g) is expected to be relatively low, but $Ni(OH)_2$(g) has higher vapor pressure at higher oxygen partial pressure. As a result, the abundance of $Ni(OH)_2$(g) at high fuel utilization (10^{-8} kmol at 800 °C in Fig. 2(b)) is 3 orders of magnitude higher than at low fuel utilization (10^{-11} kmol at 800 °C in Fig. 2(a)), at SOFC operating temperatures.

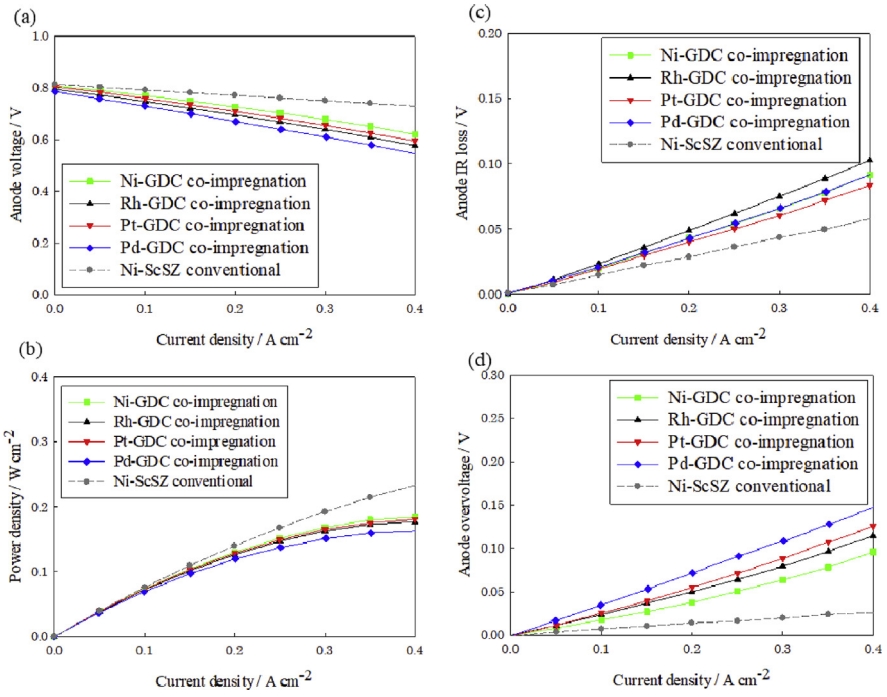

Fig. 5 – (a) Anode voltage, (b) cell power density, (c) anode IR losses, and (d) anode non-ohmic overvoltage of M-impregnated anodes (M = Ni, Rh, Pt, or Pd) and conventional Ni-cermet anodes with 95%-humidified H_2 fuel. Metal catalyst loadings are 0.167 mg-Ni cm^{-2}, 0.178 mg-Rh cm^{-2}, 0.310 mg-Pt cm^{-2}, and 0.204 mg-Pd cm^{-2}, respectively.

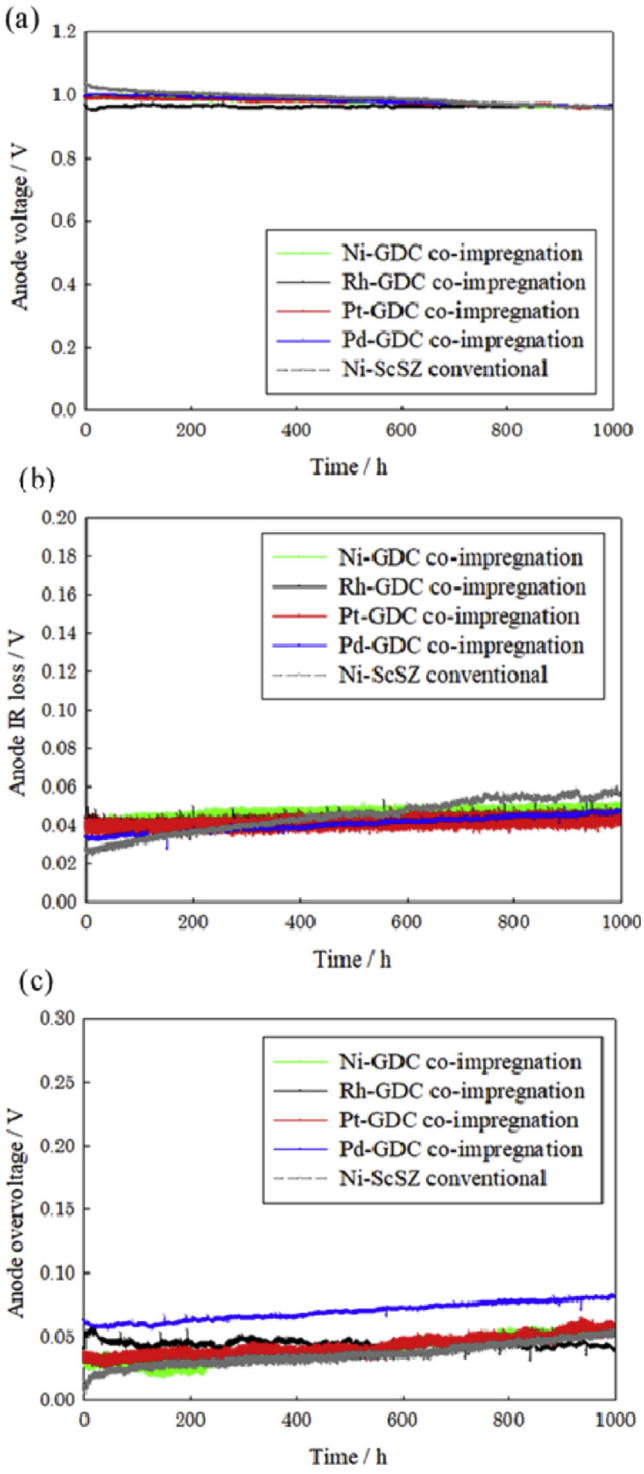

Fig. 6 – (a) Anode voltage, (b) anode IR losses, and (c) anode non-ohmic overvoltage of M-GDC co-impregnated anodes (M = Ni, Rh, Pt, or Pd) and conventional Ni-cermet anode with 3%-humidified H_2 and constant current density of 0.2 A cm^{-2}. Metal catalyst loadings are 0.167 mg-Ni cm^{-2}, 0.178 mg-Rh cm^{-2}, 0.310 mg-Pt cm^{-2}, and 0.204 mg-Pd cm^{-2}, respectively.

Sublimation of $Ni(OH)_2(g)$ could lead to deactivation of the Ni catalyst by decreasing the amount of Ni, and/or by Ni agglomeration upon reprecipitation [10,29,30].

In contrast, noble metals such as Rh, Pt, and Pd, are clearly more tolerant against oxidation according to the calculations. These metals are expected to be stable even at higher water vapor partial pressure, at high fuel utilization (Fig. 2(c)–(h)). In particular, at a typical SOFC operating temperature of 800 °C, the abundance of gaseous species of these noble metals and their compounds such as oxides is relatively low, even for a higher water vapor concentration of 95% (Fig. 2(d), (f), and (h)). In particular, the abundance of Rh-based gaseous species (Rh(g)) is below 10^{-18} kmol at 800 °C at low and high fuel utilization, as shown in Fig. 2(c) and (d). The abundance of Pt-based gaseous species (PtH(g)) is below 10^{-16} kmol at 800 °C in Fig. 2(e) and (f), and that of Pd-based gaseous species (Pd(g)) is below 10^{-11} kmol at 800 °C in Fig. 2(g) and (h). These results indicate that noble metal catalysts, especially Rh, are robust against oxidation and sublimation, even in the downstream region of SOFC systems at high fuel utilization, under which conditions Ni catalysts are easily deactivated. Thus, noble metals are applicable as alternative SOFC anode catalysts with high stability, from the thermochemical stability viewpoint.

X-ray diffraction (XRD)

Fig. 3 shows XRD patterns of an LST-GDC composite powder sintered at 1300 °C, and pre-sintered LST-GDC powders after noble metal impregnation and following thermal treatment at 1000 °C (M = Ni, Rh, Pt, or Pd). These temperatures were selected in line with the anode sintering and impregnation temperatures to simulate the phases of the impregnated anodes. After Ni, Rh, or Pd impregnation, the anode powders consist of the corresponding metal oxide phases (NiO, RhO_2, and PdO). Meanwhile, for Pt-impregnation, peaks corresponding to Pt metal were detected, which is also expected from the thermochemical calculations. Moreover, the pre-sintered LST-GDC anode powders kept their original phase peaks after M-impregnation, as well as each metal or metal oxide phase peak. This indicates no chemical reactions between each impregnated noble metal and the LST or GDC support.

Electrochemical characteristics

Figs. 4 and 5 show the I–V characteristics of four kinds of cell using the LST-GDC anode co-impregnated with Ni, Rh, Pt, or Pd, compared with a conventional Ni-ScSZ anode single cell. 3%- and 95%-humidified H_2 fuel was utilized for Figs. 4 and 5, respectively. As observed in Fig. 4(a) and (b), all of the co-impregnated anode cells exhibited comparable I–V characteristics to the conventional Ni-ScSZ cermet anode cell (~1.0 V at 0.2 A cm^{-2} with 3%-humidified H_2 fuel). Both the anode IR losses and the anode non-ohmic overvoltages decreased due to co-impregnation of noble metals with the MIEC GDC (as shown in Fig. 4(c) and (d), respectively). In contrast, Fig. 5 shows that all of the co-impregnated anode cells in this study exhibited slightly lower I–V performance compared to the conventional anode for highly-humidified H_2 fuel. This is possibly caused by decreased electronic

conductivity in the LST-GDC porous oxide backbone at higher humidity [29] and fewer reaction sites due to low loading. The anode overvoltage of the conventional anode for 95%-humidified H_2 fuel in Fig. 5(d) was slightly lower than that for 3%-humidified H_2 in Fig. 4(d). This may be because there is an optimum humidification level for anode reactions of each fuel composition [44,45], and it can take the maximum value for around 40%-humidified H_2 fuel with the same composite anode in this study [45].

Durability at high fuel utilization

In order to simulate the upstream and downstream regions of practical SOFC systems, long-term durability tests were

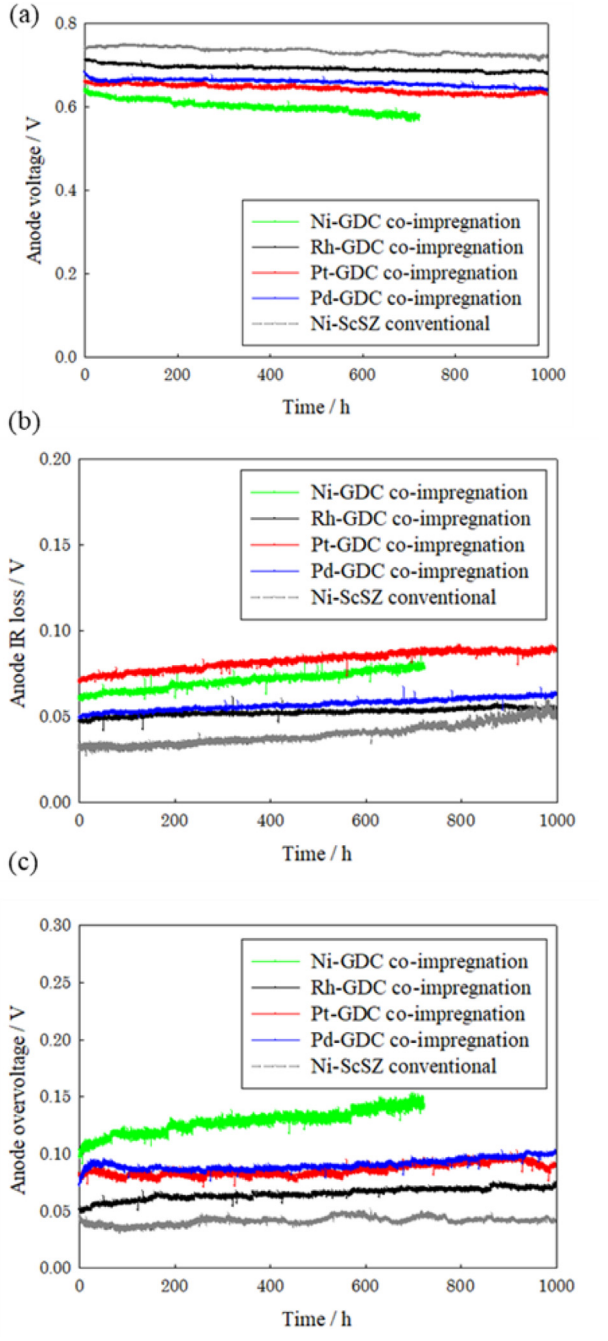

Fig. 7 – (a) Anode voltage, (b) anode IR losses, and (c) anode non-ohmic overvoltage of M-GDC co-impregnated anodes (M = Ni, Rh, Pt, or Pd) and conventional Ni-cermet anode with 95%-humidified H_2 and constant current density of 0.2 A cm^{-2}. Metal catalyst loadings are 0.167 mg-Ni cm^{-2}, 0.178 mg-Rh cm^{-2}, 0.310 mg-Pt cm^{-2}, and 0.204 mg-Pd cm^{-2}, respectively.

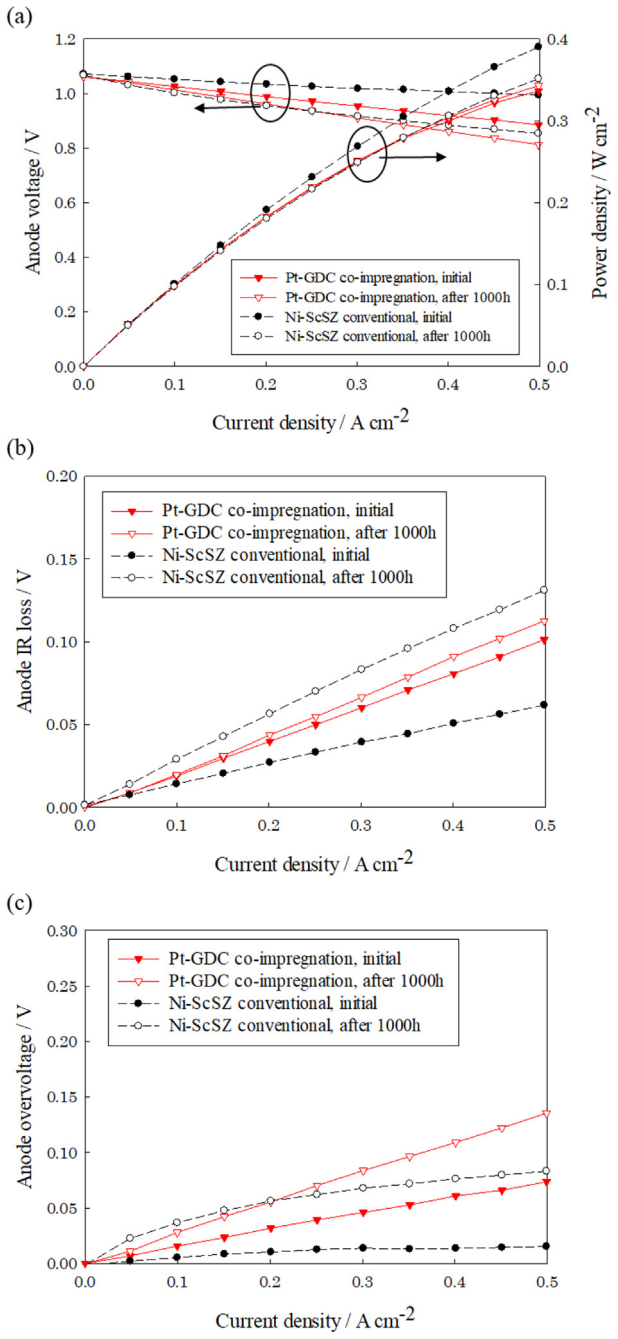

Fig. 8 – (a) Anode voltage and cell power density, (b) anode IR losses, and (c) anode non-ohmic overvoltage of Pt-GDC co-impregnated anode and conventional Ni-cermet anode with 3%-humidified H_2 before and after 1000 h operation at 0.2 A cm^{-2}. The metal catalyst loading is 0.310 mg-Pt cm^{-2}.

conducted for 1000 h at both low and high fuel utilizations (i.e. under low or high oxygen partial pressures). Changes in the anode voltages of M-GDC co-impregnated anodes with 3%- and 95%-humidified H_2 fuels are shown in Figs. 6 and 7, respectively, compared with the conventional Ni-ScSZ anode. The current density was kept constant at 0.2 A cm^{-2}. There is a slight increase in the anode non-ohmic overvoltage for low-humidified H_2 fuel (Fig. 6(c)), whilst all co-impregnated anodes were as stable as the conventional Ni-cermet anode, as shown in Fig. 6. This indicates that these materials are applicable at high hydrogen partial pressure (i.e. under strongly reducing conditions). Fig. 7 shows that for highly-humidified hydrogen fuel (U_f = 95%), whilst the anode IR losses are almost constant, the overvoltage of the Ni-GDC co-impregnated anode increases significantly, resulting in a decrease in anode voltage. The stable phase of the Ni catalyst under open circuit voltage (OCV) conditions is still metallic in the case of 95%-humidified H_2 fuel, as thermochemically expected in Fig. 2(b). However, when drawing current, the anode voltage decreases to below the Ni/NiO boundary. This is likely what leads to the deactivation of the Ni catalyst under these conditions, and indeed, the cell with the Ni-GDC co-impregnated anode lost its activity after ca. 700 h, as shown in Fig. 7 [11,29,30]. The conventional Ni-ScSZ cermet anode is well known to degrade during redox cycling. However, in this test, it displays high stability for the first 1000 h. This may be attributed to the fact that the anode voltage was kept above the Ni/NiO potential boundary. As such, conventional cermet anodes still maintained sufficient performance and stability in highly-humidified H_2 fuel as shown in Figs. 5 and 7, whilst they are known to be unstable under redox conditions [10]. This test was performed for the single cell, but in real SOFC stack systems inhomogeneous fuel supply at such high fuel utilization is expected to lead to Ni/NiO redox reactions. On the other hand, the LST-GDC anodes impregnated with Ni catalyst have good performance and stability during redox cycling [29,30], but they are unstable in highly-humidified H_2 fuel as shown in Figs. 5 and 7. The noble metal catalysts are thermochemically stable in their metallic form, suppressing any increases in the anode overvoltage compared with the Ni catalyst (Fig. 7(c)), even under highly-humidified fuel conditions. Only the LST-GDC anodes impregnated with noble-metal catalysts display acceptable performance under all the tested conditions, i.e. both during redox cycling and testing in highly-humidified H_2 fuel.

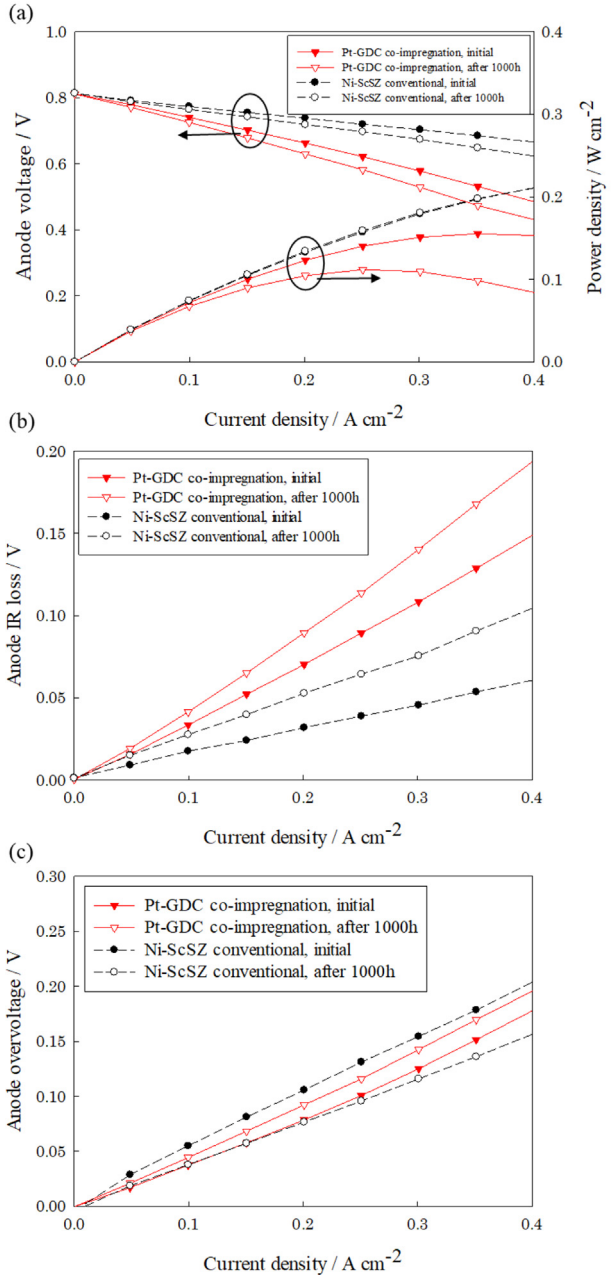

Fig. 9 – (a) Anode voltage and cell power density, (b) anode IR losses, and (c) anode non-ohmic overvoltage of Pt-GDC co-impregnated anode and conventional Ni-cermet anode with 95%-humidified H_2 before and after 1000 h operation at 0.2 A cm^{-2}. The metal catalyst loading is 0.310 mg-Pt cm^{-2}.

For comparison, changes in the anode characteristics of the Pt-GDC co-impregnated anode and the conventional Ni-ScSZ cermet anode before and after the 1000 h durability tests with 3%- and 95%-humidified H_2 fuels are shown in Figs. 8 and 9, respectively. Although some degradation was observed for these two anodes, the degradation of the conventional Ni-ScSZ cermet anode is more significant. This is attributed partially to the instability of the Ni metal backbone in conventional cermet anodes compared to the oxide backbone in the impregnated anodes.

It is therefore confirmed from both thermochemical calculations and electrochemical experimental results that noble metal catalysts are tolerant against oxidation, and are potentially useful as alternative anode catalysts, even in the downstream regions of SOFC systems at high fuel utilization. However, since a slight increase in the overvoltage of the noble metal co-impregnated anodes was detected during durability tests at both low and high humidification, the distribution of each metal catalyst was evaluated by the following microstructural observations.

Anode microstructure

The particle size distribution of the metal catalysts before and after durability tests are shown in Figs. 10–13. FIB-SEM micrographs are shown in (a-c), 3D-reconstructions of the metal catalyst nanoparticles using Amira software are shown in (d-f), and the particle size distribution is quantified in (g). Moreover, the decrease in mass of catalyst was analyzed by EDS (shown next to the ▲ symbol in the upper-right corner of (b) and (c)). The initial microstructure is shown in (a) and (d). The microstructure after durability tests with 3%-humidified H_2 fuel is shown in (b) and (e). The microstructure after durability tests with 95%-humidified H_2 fuel is shown in (c) and (f).

Fig. 10 shows that the Ni nanoparticles are highly-dispersed at the beginning, with a size of around 40 nm. After durability tests at both low and high humidification, the particle size clearly increases to more than 100 nm. Whilst similar Ni coarsening was observed under both conditions, more Ni was lost in the case of highly-humidified H_2 as measured by EDS. This loss may be caused by the sublimation of $Ni(OH)_2(g)$ due to the high vapor pressure under highly humidified conditions. Figs. 11–13 show that all of the noble metal catalyst particles also undergo coarsening during durability tests, to a similar or greater degree than Ni. However, as seen in Figs. 6 and 7, the increase in the overvoltage of the co-impregnated anodes was not so critical that the co-impregnated GDC catalyst could be still effective. In this case, the coarsening seems to be independent of the water vapor concentration. In general during sintering, coarsening may be expected to be faster for materials with a lower melting point [46]. However, here the trend was

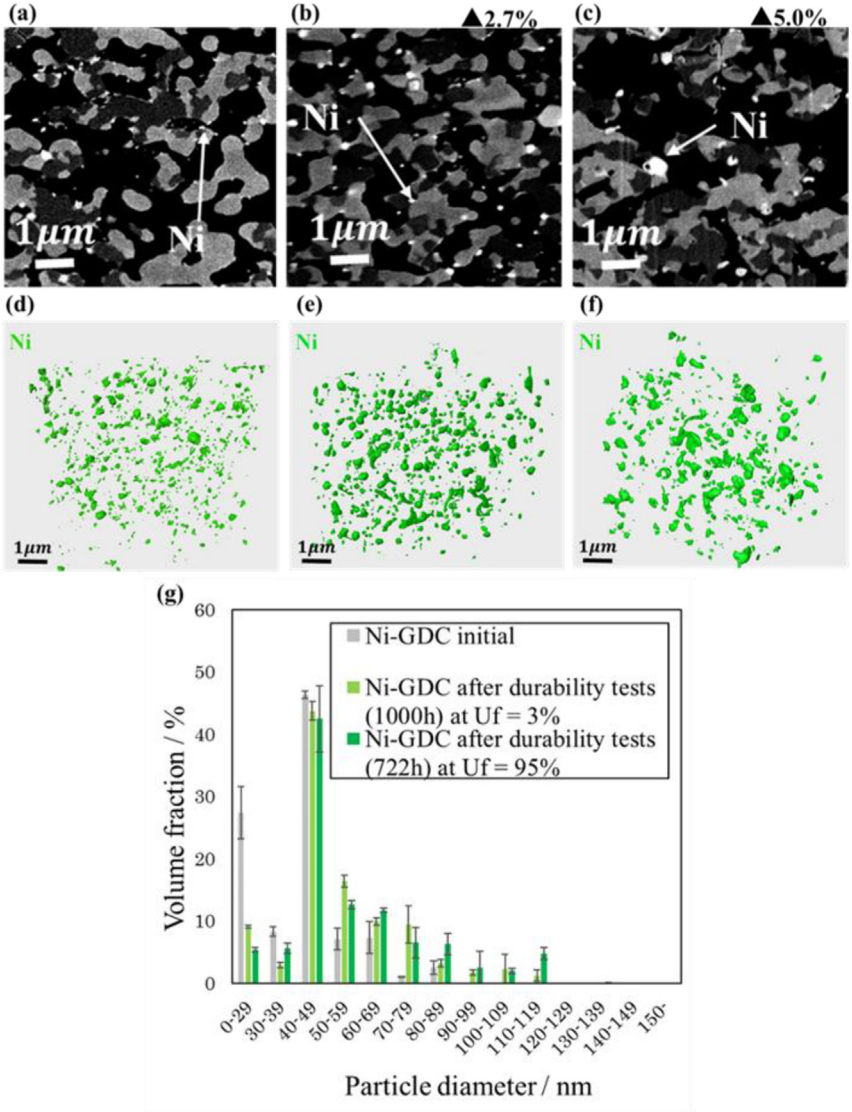

Fig. 10 – (a–c) FIB-SEM micrographs and (d–f) associated 3D-reconstruction of the Ni catalyst metal nanoparticles in Ni-GDC co-impregnated anodes: (a), (d) initial conditions; (b), (e) after 1000 h durability tests with 3%-humidified H_2; and (c), (f) after 722 h durability tests with 95%-humidified H_2. (g) Difference in Ni nanoparticle size distribution before and after durability tests. The Ni catalyst loading was 0.167 mg-Ni cm^{-2}.

different, as melting point is 1963 °C for Rh, 1768 °C for Pt, 1555 °C for Pd, and 1455 °C for Ni [47]. Ostwald ripening [48,49] and re-precipitation via sublimation [10] are other possible coarsening mechanisms. The thermochemical calculations already showed that the vapor pressure of $Ni(OH)_2(g)$ is relatively high for Ni, followed by gaseous compounds for Pd, Pt, and Rh, as shown in Fig. 2. The cohesive energy is the highest for Pt crystals (564 kJ mol^{-1}), followed by Rh (554 kJ mol^{-1}), Ni (428 kJ mol^{-1}), and Pd (376 kJ mol^{-1}) [50]. Therefore, the tendency towards coarsening of metal particles observed in this study may be governed by a complex combination of such effects. More detailed microscopic analysis by e.g. transmission electron microscopy coupled with FIB-SEM, FESEM-EDS, and XRD will be needed in a future study to analyze nanostructure and oxidation state of these catalyst particles.

Exchange current density

Fig. 14 shows different forms of exchange current density, quantifying the activities of the noble metal anodes and comparing with the conventional Ni-cermet anode [43]. The exchange current density per apparent electrode area (Fig. 14(a)), per weight of electrode catalyst metal (Fig. 14(b)), and per molar amount of electrode catalyst metal (Fig. 14(c)) are shown. Whilst all of the co-impregnated anodes show comparable I–V performance to the conventional Ni-zirconia cermet anode in Fig. 4, they exhibit lower exchange current density per apparent electrode area in Fig. 14(a). This may be caused by a slight increase in electrode overvoltage due to fewer reaction sites at such low loading, compared to the conventional Ni-based anode. Even though the Ni metal catalyst may be oxidized at high humidity, the

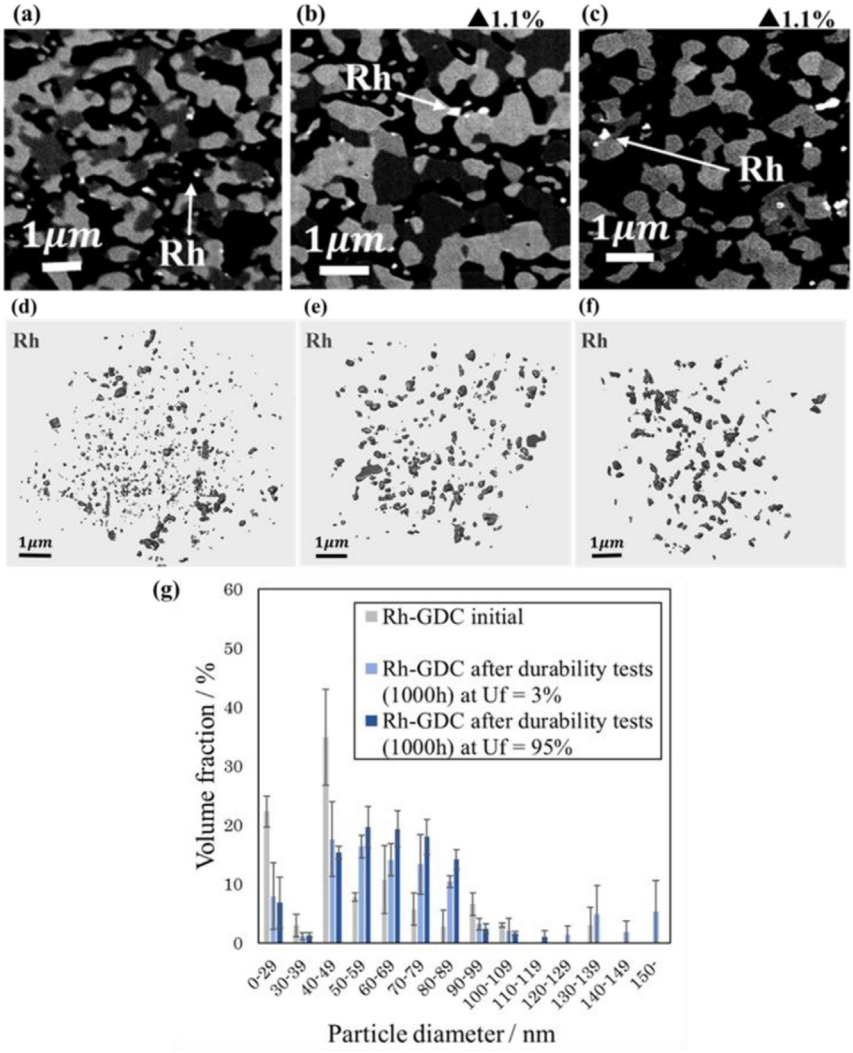

Fig. 11 – (a–c) FIB-SEM micrographs and (d–f) associated 3D-reconstruction of the Rh catalyst metal nanoparticles in Rh-GDC co-impregnated anodes: (a), (d) initial conditions; (b), (e) after 1000 h durability tests with 3%-humidified H_2; and (c), (f) after 1000 h durability tests with 95%-humidified H_2. (g) Difference in Rh nanoparticle size distribution before and after durability tests. The Ni catalyst loading was 0.178 mg-Rh cm^{-2}.

Ni-GDC co-impregnated anode still has better electrode activity than the other co-impregnated anodes, per electrode area.

Interestingly, the trend in exchange current density is different if the exchange current density is normalized to mass activity (Fig. 14(b)) and to molar activity (Fig. 14(c)). In conventional Ni-cermet anodes, much of Ni metal acts as an electron-conducting pathway, rather than as a catalyst. Therefore, the use of catalysts decorated on MIEC anodes can considerably reduce the amount of Ni used in an SOFC, as clearly shown in Fig. 14(b) and (c). Per unit mass of the catalysts (Fig. 14(b)), Ni exhibited the highest mass activity, followed by Rh, Pd, and Pt. Fig. 14(c) describes the molar activity of these catalysts, indicating that Rh is the most active anode catalyst per mole, followed by Ni, Pt, and then Pd, for H_2 fuels. This figure also clearly reveals that exchange current density per mole of the metal catalysts is much higher for impregnated-anodes than for cermet anodes. Thus, co-impregnation can considerably reduce the required amount of catalyst metals, enabling even the use of expensive noble metals in SOFCs.

Cost analysis of noble metals in SOFCs

This study reveals the applicability of noble metals such as Rh, Pt, and Pd, verified by both thermochemical calculations and electrochemical experiments. However, traditionally one of the most important advantages of SOFCs is that they are free from noble metals. Therefore, the use of noble metals is generally avoided from the viewpoint of system cost. Some researchers have previously performed cost analysis on SOFC systems [51–55]. Here we present a simple cost analysis to examine the feasibility of using low loadings of noble metal catalysts in SOFC systems.

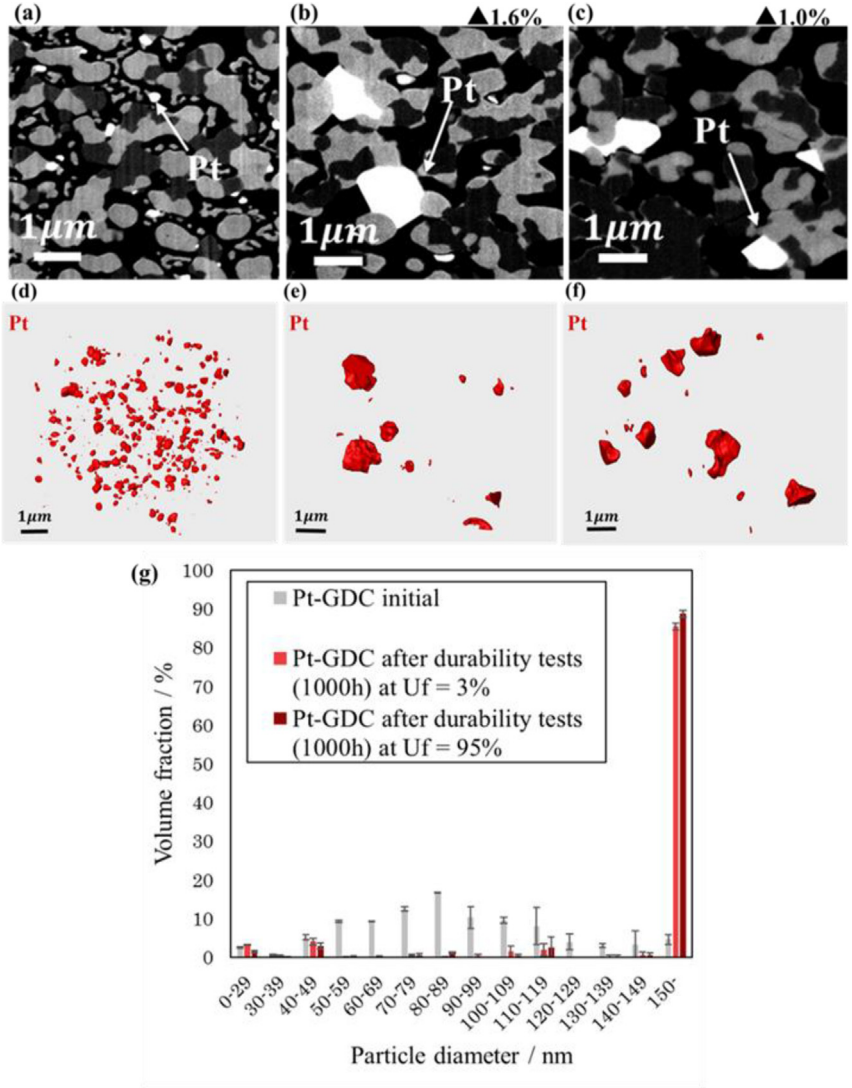

Fig. 12 – (a–c) FIB-SEM micrographs and (d–f) associated 3D-reconstruction of the Pt catalyst metal nanoparticles in Pt-GDC co-impregnated anodes: (a), (d) initial conditions; (b), (e) after 1000 h durability tests with 3%-humidified H_2; and (c), (f) after 1000 h durability tests with 95%-humidified H_2. (g) Difference in Pt nanoparticle size distribution before and after durability tests. The Pt catalyst loading was 0.310 mg-Pt cm^{-2}.

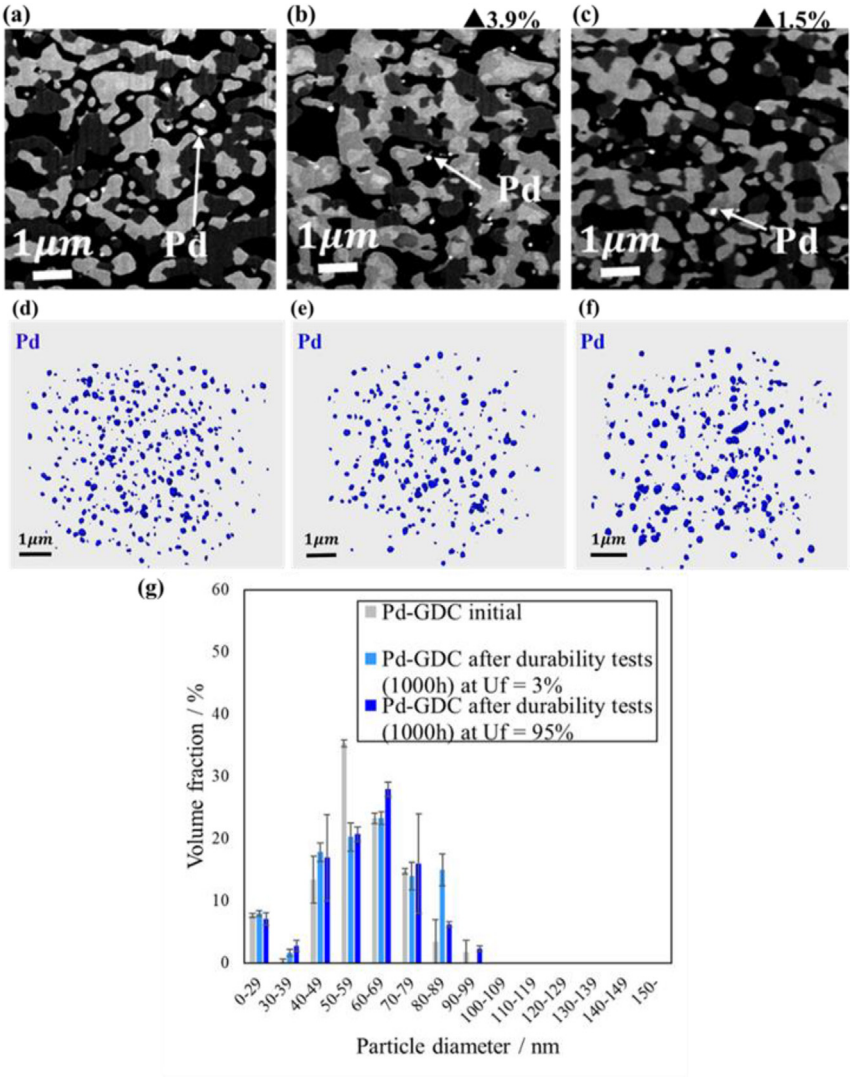

Fig. 13 – (a–c) FIB-SEM micrographs and (d–f) associated 3D-reconstruction of the Pd catalyst metal nanoparticles in Pd-GDC co-impregnated anodes: (a), (d) initial conditions; (b), (e) after 1000 h durability tests with 3%-humidified H_2; and (c), (f) after 1000 h durability tests with 95%-humidified H_2. (g) Difference in Pd nanoparticle size distribution before and after durability tests. The Pd catalyst loading was 0.204 mg-Pd cm^{-2}.

We make the assumption that the noble metal anode developed in this study will be applied only in cells in the downstream region of the system (i.e. 1/4 of the total electrode area) for higher fuel utilization. We also assume a 700 W SOFC, which is typical of the widely commercialized "Ene-Farm" residential fuel cell system in Japan [6]. If the cell voltage is 1.0 V and the average current density is 0.2 A cm^{-2} (see Fig. 4(a)), the electrode area of the noble metal anodes can be simply calculated to be:

$$700\ W/(1.0\ V \times 0.20\ A\ cm^{-2}) \times \frac{1}{4} = 8.8 \times 10^2\ cm^2$$

The impregnated catalyst metal loading in this study was 0.2–0.4 mg cm^{-2}. Given the noble metal price of $30 to $70 per gram, the raw materials cost of noble metals for one 700 W system is calculated to be:

$$(8.8 \times 10^2)cm^2 \times (0.20 \sim 0.40) \times 10^{-3}\ g\ cm^{-2} \times (\$\ 30 \sim 70)\ g^{-1} \cong \$\ 5.3 \sim 25$$

This simple cost analysis indicates that the materials cost of noble metal catalysts is just $5.3 to $25 per system. This is a small proportion of the total price of SOFC Ene-Farm systems currently available in Japan, which is currently around US$10,000.

Thus, this impregnation procedure enables us to reduce the amount of catalyst metal used in SOFC systems. This cost estimation indicates that limited use of expensive noble metals could be beneficial and cost-effective, and may have various advantages including improvements in fuel utilization, higher electric efficiency, tolerance against inhomogeneous fuel distribution within cell stacks, stability in high fuel utilization operation, improved durability in

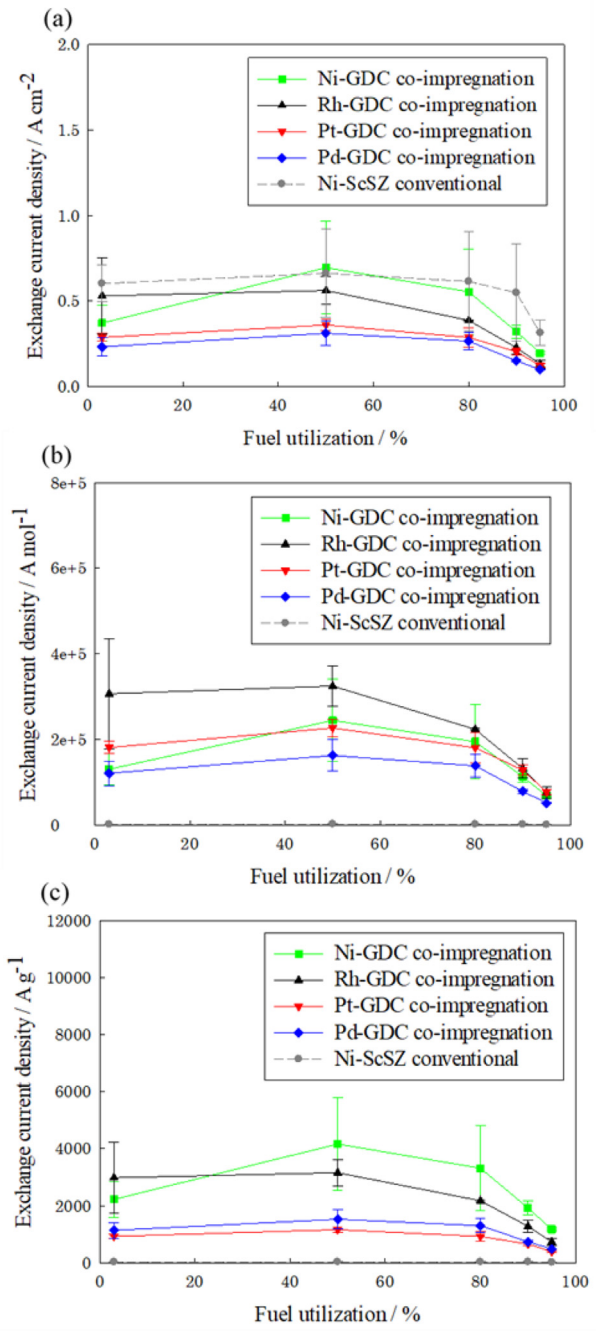

Fig. 14 – Exchange current densities of M-GDC co-impregnated anodes (M = Ni, Rh, Pt, or Pd) and conventional Ni-cermet anode with units of (a) A cm^{-2}, (b) A g^{-1}, and (c) A mo^{-1}. Metal catalyst loadings are 0.167 mg-Ni cm^{-2}, 0.178 mg-Rh cm^{-2}, 0.310 mg-Pt cm^{-2}, and 0.204 mg-Pd cm^{-2}, respectively.

shut-down and start-stop operation, and consequently more flexibility and robustness in system design.

Conclusions

Noble-metal impregnated anodes have been developed on oxide-based conducting SOFC anode backbones using electron-conducting LST and mixed ionic-electronic conducting GDC. These materials were chosen for their improved stability against redox cycling compared to the conventional Ni-zirconia cermet anode. Noble metal (Rh, Pt, or Pd) catalyst nanoparticles were decorated onto these backbones via co-impregnation with GDC to prepare thin two-dimensional cermet structure.

Conventional Ni-cermet anodes exhibited sufficient electrochemical performance even under high fuel utilization conditions, while they are known to be weak under redox conditions. The Ni-GDC co-impregnated anode with redox stability exhibits sufficient electrochemical performance but was still relatively unstable under high fuel utilization conditions. Only the co-impregnated anodes with noble metal catalysts show acceptable performances under all these conditions. These noble-metal co-impregnated anodes not only exhibit comparable I–V performance to the conventional Ni-cermet anodes, but also have better tolerance against oxidation, i.e. under high fuel utilization conditions, compared with the Ni-GDC co-impregnated anode. Whilst there are still issues to be solved such as catalyst particle agglomeration, and further improvement of electrochemical performance, these noble-metal co-impregnated anodes with stable backbone structure could be a promising alternative robust anode for high fuel utilization operation of SOFC systems.

Compared to the conventional cermet anodes, the co-impregnated anodes achieve considerably high mass activity and high molar activity of catalysts, for both Ni and noble metals. This enables us to effectively improve catalyst utilization and to drastically reduce the amount of catalysts used in the cells, and thus their materials cost. Whilst additional costs should also be taken into account in using alternative materials such as LST, and in applying extra manufacturing processes such as impregnation, a simple cost analysis in this study suggested that the use of impregnated noble metal catalysts is feasible, as long as the noble metal loading is relatively low.

Acknowledgements

Financial support from the Center of Innovation (COI) Program by the Japan Science and Technology Agency (JST) is gratefully acknowledged.

REFERENCES

[1] Minh NQ. Ceramic fuel cells. J Am Ceram Soc 1993;76:563–88. https://doi.org/10.1111/j.1151-2916.1993.tb03645.x.
[2] Steele BCH, Heinzel A. Materials for fuel-cell technologies. Nature 2001;414:345–52. https://doi.org/10.1038/35104620.
[3] Singhal SC, Kendall K. In: Singhal SC, Kendall K, editors. High temperature solid oxide fuel cells. Elsevier; 2003 (ISBN 978-0-080-50808-5).
[4] Larminie J, Dicks A. Fuel cell systems explained. 2nd ed. Wiley; 2003 (ISBN 978-0-470-84857-9).
[5] Vielstich W, Lamm A, Gasteiger HA, editors. Handbook of fuel cells: fundamentals, technology, and applications. Wiley; 2003 (ISBN 978-0-471-49926-8).

[6] Sasaki K, Li HW, Hayashi A, Yamabe J, Ogura T, Lyth SM, editors. Hydrogen energy engineering: a Japanese perspective. Springer; 2016 (ISBN 978-4-431-56042-5).

[7] Klemensϕ T, Mogensen M. Ni–YSZ solid oxide fuel cell anode behavior upon redox cycling based on electrical characterization. J Am Ceram Soc 2007;90:3582–8. https://doi.org/10.1111/j.1551-2916.2007.01909.x.

[8] Holzer L, Iwanschitz B, Hocker Th, Munch B, Preatat M, Wiedenmann D, Vogt U, Holtappels P, Sfeir J, Mai A, Graule TH. Microstructure degradation of cermet anodes for solid oxide fuel cells: quantification of nickel grain growth in dry and in humid atmospheres. J Power Sources 2011;196:1279–94. https://doi.org/10.1016/j.jpowsour.2010.08.017.

[9] Holzer L, Iwanschitz B, Hocker Th, Keller L, Pecgo O, Sartoris G, Gasser Ph, Muench B. Redox cycling of Ni–YSZ anodes for solid oxide fuel cells: influence of tortuosity, constriction and percolation factors on the effective transport properties. J Power Sources 2013;242:179–94. https://doi.org/10.1016/j.jpowsour.2013.05.047.

[10] Hanasaki M, Uryu C, Daio T, Kawabata T, Tachikawa Y, Lyth SM, Shiratori Y, Taniguchi S, Sasaki K. SOFC durability against standby and shutdown cycling. J Electrochem Soc 2014;161:F850–60. https://doi.org/10.1149/2.0421409jes.

[11] Kawasaki T, Sugimoto J, Tachikawa Y, Shiratori Y, Taniguchi S, Sasaki K. Oxidation-Induced degradation of SOFC Ni anodes at high fuel utilizations. ECS Trans 2015;68:1345–52. https://doi.org/10.1149/06801.1345ecst.

[12] Liang B, Zhang S, Zhang Z, Lu B, Lu S, Kendall M, Ni M. Dimensional analysis of Ni-NiO grains at anode/electrolyte interface for SOFC during redox reaction. Int J Appl Ceram Technol 2017;14:543–9. https://doi.org/10.1111/ijac.12667.

[13] Marina OA, Canfield NL, Stevenson JW. Thermal, electrical, and electrocatalytical properties of lanthanum-doped strontium titanate. Solid State Ionics 2002;149:21–8. https://doi.org/10.1016/S0167-2738(02)00140-6.

[14] Obara H, Yamamoto A, Lee CH, Kobayashi K, Matsumoto A, Funahashi R. Thermoelectric properties of Y-doped polycrystalline $SrTiO_3$. Jpn J Appl Phys 2004;43:L540–2. https://doi.org/10.1143/JJAP.43.L540.

[15] Li X, Zhao H, Shen W, Gao F, Huang X, Li Y, Zhu Z. Synthesis and properties of Y-doped $SrTiO_3$ as an anode material for SOFCs. J Power Sources 2007;166:47–52. https://doi.org/10.1016/j.jpowsour.2007.01.008.

[16] Wang Z, Mori M, Itoh T. Thermal expansion properties of $Sr_{1-x}La_xTiO_3$ ($0 \leqslant x \leqslant 0.3$) perovskites in oxidizing and reducing atmospheres. J Electrochem Soc 2010;157:B1783–9. https://doi.org/10.1149/1.3481458.

[17] Wang Z, Mori M. Sintering characteristics and electrical conductivity of $(Sr_{1-x}La_x)TiO_3$ synthesized by the citric acid method. J Fuel Cell Sci Technol 2011;8, 051018. https://doi.org/10.1115/1.4003993.

[18] Ma Q, Tietz F. Comparison of Y and La-substituted $SrTiO_3$ as the anode materials for SOFCs. Solid State Ionics 2012;225:108–12. https://doi.org/10.1016/j.ssi.2012.03.048.

[19] Kim G, Gross MD, Wang W, Vohs JM, Gorte RJ. SOFC anodes based on LST–YSZ composites and on $Y_{0.04}Ce_{0.48}Zr_{0.48}O_2$. J Electrochem Soc 2008;155:B360–6. https://doi.org/10.1149/1.2840473.

[20] Irvine JTS, Neagu D, Verbraeken MC, Chatzichristodoulou C, Graves C, Mogensen MB. Evolution of the electrochemical interface in high-temperature fuel cells and electrolysers. Nature Energy 2016;1:15014. https://doi.org/10.1038/nenergy.2015.14.

[21] Yoo KB, Choi GM. Performance of La-doped strontium titanate (LST) anode on $LaGaO_3$-based SOFC. Solid State Ionics 2009;180:867–71. https://doi.org/10.1016/j.ssi.2009.02.013.

[22] Yoo KB, Choi GM. LST–GDC composite anode on $LaGaO_3$-based solid oxide fuel cell. Solid State Ionics 2011;192:515–8. https://doi.org/10.1016/j.ssi.2010.06.048.

[23] Chen G, Kishimoto H, Yamaji K, Kuramoto K, Horita T. Effect of interaction between A-site deficient LST and ScSZ on electrochemical performance of SOFC. J Electrochem Soc 2015;162:F223–8. https://doi.org/10.1149/2.0131503jes.

[24] Shen X, Sasaki K. Highly redox-resistant solid oxide fuel cell anode materials based on La-doped $SrTiO_3$ by catalyst impregnation strategy. J Power Sources 2016;320:180–7. https://doi.org/10.1016/j.jpowsour.2016.04.111.

[25] Shen X, Sasaki K. Robust SOFC anode materials with La-doped $SrTiO_3$ backbone structure. Int J Hydrog Energy 2016;41:17044–52. https://doi.org/10.1016/j.ijhydene.2016.08.024.

[26] Tsekouras G, Neagu D, Irvine JTS. Step-change in high temperature steam electrolysis performance of perovskite oxide cathodes with exsolution of B-site dopants. Energy Environ Sci 2013;6:256–66. https://doi.org/10.1039/C2EE22547F.

[27] Neagu D, Oh TS, Miller DN, Menard H, Bukhari SM, Gamble SR, Gorte RJ, Vohs JM, Irvine JTS. Nano-socketed nickel particles with enhanced coking resistance grown in situ by redox exsolution. Nat Commun 2015;6:8120. https://doi.org/10.1038/ncomms9120.

[28] Shen X, Chen T, Bishop SR, Perry NH, Tuller HL, Sasaki K. Redox cycling induced Ni exsolution in $Gd_{0.1}Ce_{0.8}Ni_{0.1}O_2$ - $(Sr_{0.9}La_{0.1})_{0.9}Ti_{0.9}Ni_{0.1}O_3$ composite solid oxide fuel cell anodes. J Power Sources 2017;370:122–30. https://doi.org/10.1016/j.jpowsour.2017.10.009.

[29] Futamura S, Tachikawa Y, Matsuda J, Lyth SM, Shiratori Y, Taniguchi S, Sasaki K. Alternative Ni-impregnated mixed ionic-electronic conducting anode for SOFC operation at high fuel utilization. J Electrochem Soc 2017;164:F3055–63. https://doi.org/10.1149/2.0071710jes.

[30] Futamura S, Tachikawa Y, Matsuda J, Lyth SM, Shiratori Y, Taniguchi S, Sasaki K. Alternative SOFC anode materials with ion– and electron–conducting backbones for higher fuel utilization. ECS Trans 2017;78:1179–87. https://doi.org/10.1149/07801.1179ecst.

[31] Saeki MJ, Uchida H, Watanabe M. Noble metal catalysts highly-dispersed on Sm-doped ceria for the application to internal reforming solid oxide fuel cells operated at medium temperature. Catal Lett 1994;26:149–57. https://doi.org/10.1007/BF00824040.

[32] Liguras DK, Kondarides DI, Verykios XE. Production of hydrogen for fuel cells by steam reforming of ethanol over supported noble metal catalysts. Appl Catal B Environ 2003;43:345–54. https://doi.org/10.1016/S0926-3373(02)00327-2.

[33] Peela NR, Kunzru D. Oxidative steam reforming of ethanol over Rh based catalysts in a micro-channel reactor. Int J Hydrog Energy 2011;36:3384–96. https://doi.org/10.1016/j.ijhydene.2010.12.091.

[34] Takeguchi T, Kikuchi R, Yano T, Eguchi K, Murata K. Effect of precious metal addition to Ni-YSZ cermet on reforming of CH_4 and electrochemical activity as SOFC anode. Catal Today 2003;84:217–22. https://doi.org/10.1016/S0920-5861(03)00278-5.

[35] McIntosh S, Vohs JM, Gorte RJ. Effect of precious-metal dopants on SOFC anodes for direct utilization of hydrocarbons. Electrochem Solid State Lett 2003;6:A240–3. https://doi.org/10.1149/1.1613231.

[36] Kim JS, Wieder NL, Abraham AJ, Cargnello M, Fornasiero P, Gorte RJ, Vohs JM. Highly active and thermally stable core-shell catalysts for solid oxide fuel cells. J Electrochem Soc 2011;158:B596–600. https://doi.org/10.1149/1.3571039.

[37] Kim JS, Nair VV, Vohs JM, Gorte RJ. A study of the methane tolerance of LSCM–YSZ composite anodes with Pt, Ni, Pd and ceria catalysts. Scripta Mater 2011;65:90–5. https://doi.org/10.1016/j.scriptamat.2010.06.016.
[38] Park K, Lee S, Bae G, Bae J. Performance analysis of Cu, Sn and Rh impregnated NiO/CGO91 anode for butane internal reforming SOFC at intermediate temperature. Renew Energy 2015;83:483–90. https://doi.org/10.1016/j.renene.2015.04.070.
[39] Sugimoto J, Futamura S, Kawabata T, Lyth SM, Shiratori Y, Taniguchi S, Sasaki K. Ru-based SOFC anodes: preparation, performance, and durability. Int J Hydrog Energy 2017;42:6950–64. https://doi.org/10.1016/j.ijhydene.2017.01.028.
[40] Sasaki K, Teraoka Y. Equilibria in fuel cell gases I. Equilibrium compositions and reforming conditions. J Electrochem Soc 2003;150:A878–84. https://doi.org/10.1149/1.1577337.
[41] Sasaki K, Teraoka Y. Equilibria in fuel cell gases II. The C-H-O ternary diagrams. J Electrochem Soc 2003;150:A885–8. https://doi.org/10.1149/1.1577338.
[42] Sasaki K, Wurth JP, Gschwend R, Gödickemeier M, Gauckler LJ. Microstructure-property relations of solid oxide fuel cell cathodes and current collectors cathodic polarization and ohmic resistance. J Electrochem Soc 1996;143:530–43. https://doi.org/10.1149/1.1836476.
[43] Hosoi T, Yonekura T, Sunada K, Sasaki K. Exchange current density of SOFC electrodes: theoretical relations and partial pressure dependencies rate-determined by electrochemical reactions. J Electrochem Soc 2015;162:F136–52. https://doi.org/10.1149/2.0561501jes.
[44] Jiang SP, Ramprakash Y. H_2 oxidation on Ni/Y–TZP cermet electrodes – polarisation behavior. Solid State Ionics 1999;116:145–56. https://doi.org/10.1016/S0167-2738(98)00269-0.
[45] Yonekura T, Tachikawa Y, Yoshizumi T, Shiratori Y, Ito K, Sasaki K. Exchange current density of solid oxide fuel cell electrodes. ECS Trans 2011;35:1007–14. https://doi.org/10.1149/1.3570081.
[46] Kingery WD, Bowen HK, Uhlmann DR. Introduction to ceramics. 2nd ed. Wiley; 1976 (ISBN 978-0-471-47860-7).
[47] Lide DR. CRC handbook of chemistry and physics. 85th ed. CRC Press; 2004 (ISBN 978-0-849-30485-9).
[48] Ouyang R, Liu JX, Li WX. Atomistic theory of ostwald ripening and disintegration of supported metal particles under reaction conditions. J Am Chem Soc 2013;135:1760–71. https://doi.org/10.1021/ja3087054.
[49] Hansen TW, Delariva AT, Challa SR, Datye AK. Sintering of catalytic nanoparticles: particle migration or ostwald ripening? Acc Chem Res 2013;46:1720–30. https://doi.org/10.1021/ar3002427.
[50] Kittel C, editor. Introduction to solid state physics. 8th ed. Wiley; 2005 (ISBN 978-0-471-41526-8).
[51] Omosun AO, Bauen A, Brandon NP, Adjiman CS, Hart D. Modelling system efficiencies and costs of two biomass-fuelled SOFC systems. J Power Sources 2004;131:96–106. https://doi.org/10.1016/j.jpowsour.2004.01.004.
[52] Anghilante R, Colomar D, Brisse A, Marrony M. Bottom-up cost evaluation of SOEC systems in the range of 10–100 MW. Int J Hydrog Energy 2018;43:20309–22. https://doi.org/10.1016/j.ijhydene.2018.08.161.
[53] Zhu H, Kee RJ. Thermodynamics of SOFC efficiency and fuel utilization as functions of fuel mixtures and operating conditions. J Power Sources 2006;161:957–64. https://doi.org/10.1016/j.jpowsour.2006.05.006.
[54] Hao Y, Goodwin DG. Efficiency and fuel utilization of methane-powered single-chamber solid oxide fuel cells. J Power Sources 2008;183:157–63. https://doi.org/10.1016/j.jpowsour.2008.04.072.
[55] Oryshchyn D, Harun NF, Tucker D, Bryden KM, Shadle L. Fuel utilization effects on system efficiency in solid oxide fuel cell gas turbine hybrid systems. Appl Energy 2018;228:1953–65. https://doi.org/10.1016/j.apenergy.2018.07.004.